Nanotechnology **22** (2011) 455703 (9pp) doi:10.1088/0957-4484/22/45/455703

Uncertainty quantification in nanomechanical measurements using the atomic force microscope*

Ryan Wagner[1,2], Robert Moon[2,3,4], Jon Pratt[5], Gordon Shaw[5] and Arvind Raman[1,2]

[1] School of Mechanical Engineering, Purdue University, West Lafayette, IN 47907, USA
[2] Birck Nanotechnology Center, Purdue University, West Lafayette, IN 47907, USA
[3] School of Materials Engineering, Purdue University, West Lafayette, IN 47907, USA
[4] Forest Products Laboratory, US Forest Service, Madison, WI 53726, USA
[5] Physical Measurement Laboratory, National Institute of Standards and Technology, Gaithersburg, MD 20899, USA

Received 18 May 2011, in final form 19 September 2011
Published 13 October 2011
Online at stacks.iop.org/Nano/22/455703

Abstract
Quantifying uncertainty in measured properties of nanomaterials is a prerequisite for the manufacture of reliable nanoengineered materials and products. Yet, rigorous uncertainty quantification (UQ) is rarely applied for material property measurements with the atomic force microscope (AFM), a widely used instrument that can measure properties at nanometer scale resolution of both inorganic and biological surfaces and nanomaterials. We present a framework to ascribe uncertainty to local nanomechanical properties of any nanoparticle or surface measured with the AFM by taking into account the main uncertainty sources inherent in such measurements. We demonstrate the framework by quantifying uncertainty in AFM-based measurements of the transverse elastic modulus of cellulose nanocrystals (CNCs), an abundant, plant-derived nanomaterial whose mechanical properties are comparable to Kevlar fibers. For a single, isolated CNC the transverse elastic modulus was found to have a mean of 8.1 GPa and a 95% confidence interval of 2.7–20 GPa. A key result is that multiple replicates of force–distance curves do not sample the important sources of uncertainty, which are systematic in nature. The dominant source of uncertainty is the nondimensional photodiode sensitivity calibration rather than the cantilever stiffness or Z-piezo calibrations. The results underscore the great need for, and open a path towards, quantifying and minimizing uncertainty in AFM-based material property measurements of nanoparticles, nanostructured surfaces, thin films, polymers and biomaterials.

S Online supplementary data available from stacks.iop.org/Nano/22/455703/mmedia

(Some figures in this article are in colour only in the electronic version)

1. Introduction

Quantifying the material properties of nanomaterials is a major challenge in the development of reliable nanoengineered products and materials. However, the mechanical properties of nanostructures reported in the literature at best give the mean and standard deviation of experimental replicates without regard to the underlying uncertainty. As a consequence it can be difficult to compare measurements between different groups, instruments and techniques. This is a serious impediment to the development of reliable nanoengineered materials and products and can only be resolved by taking into account the relevant uncertainties that arise from the physical limits of the instrument, the physical limits on calibration uncertainty, data processing and mathematical models used for extracting these properties.

Atomic force microscopy (AFM) [1] force measurements using force–distance curves is a commonly used technique

* This work is a partial contribution of the USDA Forest Service and NIST, agencies of the US government, and is not subject to copyright.

 © 2011 IOP Publishing Ltd Printed in the UK & the USA

to measure the mechanical properties of a wide variety of materials including nanostructures such as monolayer graphene [2], viruses [3], cellulose nanocrystals [4], carbon nanotubes [5], pharmaceutical particles [6], zinc oxide nanowires [7, 8, 10], aluminum nitride nanotubes [9] and living cells [11]. The force sensor in an AFM consists of a sharp tip (typical radius of curvature of 10 nm) mounted on a cantilever (typically 200–300 μm by 20–35 μm by 0.5–3 μm). The tip–sample distance is controlled by means of a piezoelectric actuator (Z-piezo) which displaces the cantilever with respect to the sample or vice versa. The deflection of the cantilever is monitored by a detection system; typically a laser and photodiode. Several AFM modes can measure material properties. These modes include force modulation AFM [12], contact resonance AFM [13] and force–displacement AFM [14]. All of these modes involve the extraction of the tip–sample interaction force as a function of the distance between the tip and the sample. Once this relationship is extracted, a model can be fitted to the interaction force and material properties can be estimated [14]. For objects with nanoscale dimensions, AFM is one of the few methods with both the displacement and force resolution to investigate their mechanical properties. However, these measurements are often indirect and careful analysis of uncertainty propagation is required.

The traceability of AFM calibration parameters, such as piezoelectric stage actuation and cantilever stiffness, to SI standards has been addressed in the literature [15–17]. However, an overall framework for analyzing uncertainties in a mechanical property measured using AFM, for example the nanoscale elastic modulus or work of adhesion, has not yet been explored. Given there are in excess of a 1000 published works on the use of force–displacement based AFM measurements the need to lay a framework for analyzing uncertainties in these measured quantities is clear.

Cellulose nanocrystals (CNCs) are crystalline, rod-like shaped particles (2–20 nm in width, 50–4000 nm in length) that can be extracted from a variety of plants and marine animals via acid hydrolysis [18, 19]. CNCs have a high aspect ratio, good mechanical properties, low density (1.6 g cm^{-3}) and a reactive surface of –OH side groups that facilitates grafting chemical species to achieve different surface properties. The axial moduli of CNCs have been measured to be approximately 150 GPa [18, 19]; however, their transverse elastic properties are poorly understood due to the difficulty of measurement [4, 20]. The transverse CNC elastic properties are important for particle–particle and particle–matrix load transfer within reinforced polymer matrix composites and neat films, both of which are potential applications of CNCs.

The current work applies uncertainty analysis techniques [21] to the measurement of elastic and adhesive properties of nanoscale materials with AFM. A framework is developed that can be used by the AFM community to estimate uncertainties in sample properties (such as elastic modulus or work of adhesion) by careful consideration of calibration uncertainties, instrument uncertainties and model uncertainties. A data reduction equation (DRE) for the extraction of a given material property is presented in terms of independent variables, the uncertainties associated with the independent variables are analyzed and the dominant uncertainties are propagated through the DRE. This framework is demonstrated by measuring the transverse elastic modulus and work of adhesion of CNCs using force–displacement (F–Z) curves in AFM. CNCs are an ideal case study because of their potential for use in a wide variety of emerging applications such as stimuli-responsive nanocomposites [22], and transparent and high gas barrier films [23]. F–Z curve analysis of CNCs are presented with a specific focus on uncertainty quantification (UQ) methodology. Control experiments are performed on samples with known properties (polystyrene spheres, described in the supplementary materials). The result of the case study is that the probability distribution of the measured transverse elastic modulus (E) of an isolated CNC has a mean value of 8.1 GPa and at 95% confidence interval (CI) of 2.7–20 GPa and the dominant source of uncertainty in E is uncertainty in the nondimensional photodiode sensitivity (m) which accounts for 90% of the variance in E. Not only does this work underscore the rather large uncertainty that is intrinsic to elastic modulus measurements of nanoparticles using the AFM, it also highlights the key quantity that instrument developers need to focus on in order to reduce the uncertainty in such measurements.

2. Theory

2.1. Review of material property extraction process with AFM F–Z curves

The methodology for extracting material properties from AFM F–Z curves is well known [14]. First, the photodiode and Z-piezo voltages must be converted into forces and displacements by a series of calibration parameters. Next, these forces and displacements must be converted into forces and distances. Finally, this force–distance data must be fitted to a material model that contains as a parameter the material property of interest.

Because of the central role calibration parameters will take in the following discussion it is worthwhile to review the calibration parameters present in a typical AFM experiment.

(1) The Z-piezo voltage, Z_V (volts), must be converted into Z-piezo displacement, Z_{nm} (nm). This can be accomplished by scanning a height standard as shown in figure 1(A) or by calibrating the piezoelectric directly with an interferometer. This calibration factor is called the Z-piezo sensitivity (C_Z).

(2) The photodiode voltage, δ_V (volts), must be converted into cantilever deflection, δ_{nm} (nm). This can be accomplished by performing an F–Z curve on a stiff sample as shown in figure 1(B) or by matching the thermal oscillations of the cantilever with the cantilever stiffness [24]. This calibration factor is called the photodiode sensitivity (C_L). To simplify the uncertainty analysis we will use a parameter we call the nondimensional photodiode sensitivity (m), which is the volts of Z-piezo input voltage per volt of photodiode output voltage on a stiff sample. The nondimensional photodiode sensitivity is related to

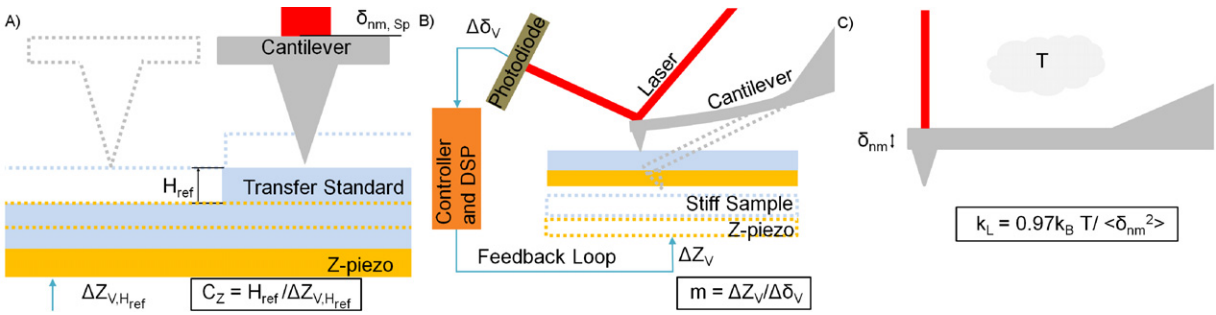

Figure 1. Schematic of calibration experiments. (A) Transfer standard for Z-piezo motion calibration, $C_Z = H_{ref}/\Delta Z_{V,H_{ref}}$, where C_Z is the Z-piezo sensitivity, H_{ref} is the height of the transfer standard and $\Delta Z_{V,H_{ref}}$ is the measured Z-piezo voltage corresponding to the height standard. (B) This shows the calibration scheme for the nondimensional photodiode sensitivity, $m = \Delta Z_V/\Delta\delta_V$, where ΔZ_V is the change in Z-piezo voltage and $\Delta\delta_V$ is the corresponding change in photodiode voltage on a sample that is stiff relative to the sample to be measured in the experiment. (C) This shows the set-up for a thermal calibration of cantilever stiffness, k_L. The thermal oscillations of the cantilever, δ_{nm}, are measured at a known absolute temperature, T. The mean squared deflection of the cantilever, $\langle\delta_{nm}^2\rangle$, is related to the cantilever stiffness though T and Boltzmann's constant, k_B.

the photodiode sensitivity by the equation $m = C_L/C_Z$. This is done to avoid correlated uncertainty terms in the uncertainty propagation equation and is discussed in additional detail in section 2.3.

(3) The cantilever deflection needs to be converted into tip–sample force, F. This can be accomplished by several methods including Sader's method [25] and the thermal tuning method [26, 27] as shown in figure 1(C). This calibration factor is called the cantilever stiffness (k_L). However, the AFM cantilever is rarely positioned parallel to the surface. It is usually inclined at some angle (θ) relative to the surface. This leads to an effective stiffening of the cantilever. A cantilever tilt correction factor (α) is given as $\alpha = 1/\cos^2(\theta)$ [28].

After these calibrations are performed, it is possible to convert the voltages of the AFM system into a series of forces (F) and tip–sample distances (d, $d < 0$ is also called the gap and $d > 0$ is also called the indentation). Tip–sample distance is related to Z-piezo displacement and cantilever deflection by the equation $d = Z_{nm} - \delta_{nm}$. Next, the F–d curve is fitted to a mathematical model that contains relevant system properties, such as elastic modulus and work of adhesion. The mechanical properties are then those that provide the best fit to the experimental F–d data (see the supplement for details, available at stacks.iop.org/Nano/22/455703/mmedia). For the case of CNCs the Derjaguin–Müller–Toporov (DMT) contact model between a spherical AFM tip and a cylindrical CNC was used to fit the experimental F–d curves to extract the local elastic modulus and work of adhesion.

2.2. Data reduction equation

The process of extracting material properties from AFM F–Z curves can be thought of as constructing a DRE. The inputs to the DRE are the calibration parameters, the model parameters, the photodiode voltage and the Z-piezo voltage. This DRE converts these inputs into an estimate of the material property of interest, for example the elastic modulus.

The DRE for computing the elastic modulus consists of $2n+9$ independent inputs, where n is the number of data points used in the curve fitting algorithm. The output of the DRE is the elastic modulus (E). The DRE for E has the form

$$E = f_1(Z_{V,1}, \ldots, Z_{V,n}, \delta_{V,1}, \ldots, \delta_{V,n}, C_Z, m, k_L, \alpha, R_V, R_{tip}, E_{tip}, \nu_{tip}, \nu) \quad (1)$$

where $Z_{V,i}$ and $\delta_{V,i}$ are the data points in the F–Z curve. The other input parameters are discussed in section 2.3. Similarly, the DRE for the work of adhesion (W) in terms of $2n + 6$ independent variables is given as

$$W = f_2(Z_{V,1}, \ldots, Z_{V,n}, \delta_{V,1}, \ldots, \delta_{V,n}, C_Z, m, k_L, \alpha, R_V, R_{tip}) \quad (2)$$

A closed-form analytic solution to these equations cannot be provided. Instead, a numerical algorithm is constructed to approximate equations (1) and (2). The construction of this algorithm for the specific case of CNCs is discussed in the supplement (available at stacks.iop.org/Nano/22/455703/mmedia).

2.3. Input uncertainties

The quantities directly observable in an AFM F–Z experiment are the voltage applied to the Z-piezo (Z_V) and the voltage output of the photodiode detector (δ_V). To convert these observables into force and distance several calibration parameters are needed: Z-piezo sensitivity (C_Z), nondimensional photodiode sensitivity (m), cantilever stiffness (k_L) and cantilever tilt angle correction factor (α). All of these factors influence the output of the curve fitting procedure, which can be related to E. The parameters E_{tip}, ν_{tip}, R_{tip}, ν and R_V are inputs into the model function to determine E. Figure 3 overviews how uncertainty propagates from this collection of input parameters to the output of elastic modulus. This methodology is discussed in additional detail in the supplement (available at stacks.iop.org/Nano/22/455703/mmedia).

Before performing the F–Z experiment the values and uncertainties of the above calibration parameters must be determined. The Z-piezo sensitivity (C_Z) was determined by scanning an H8 calibration grating provided by nanosensors that is shown in figure 2(A). The grating was calibrated by the

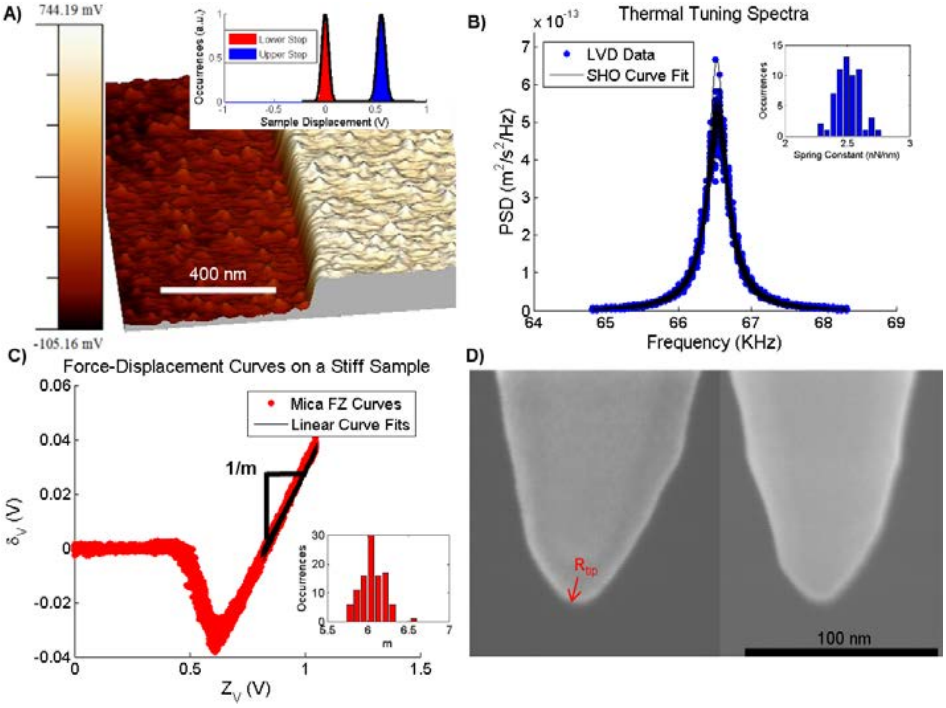

Figure 2. (A) AFM topography image of the step edge of the H8 sample provided by Nanosensors GmbH for Z-piezo calibration. Inset is the distribution of height measurement in volts. The actual height is 7.9 ± 1.1 nm. (B) Thermal tuning spectra of AFM cantilever. These curves are used for calibration of cantilever stiffness. Inset shows the histogram of 60 results for cantilever stiffness obtained while varying the vibrometer laser spot over the approximate location of the cantilever tip. (C) Force–displacement curves on a stiff sample. These curves are used for calibration of the nondimensional photodiode sensitivity, m, which is defined as the inverse of the slope (volts/volts) of the deflection versus Z-piezo displacement curve in the repulsive regime of interaction. Inset shows the histogram for 103 results for the fitting of m. (D) Scanning electron microscope images of AFM tip before and after scanning.

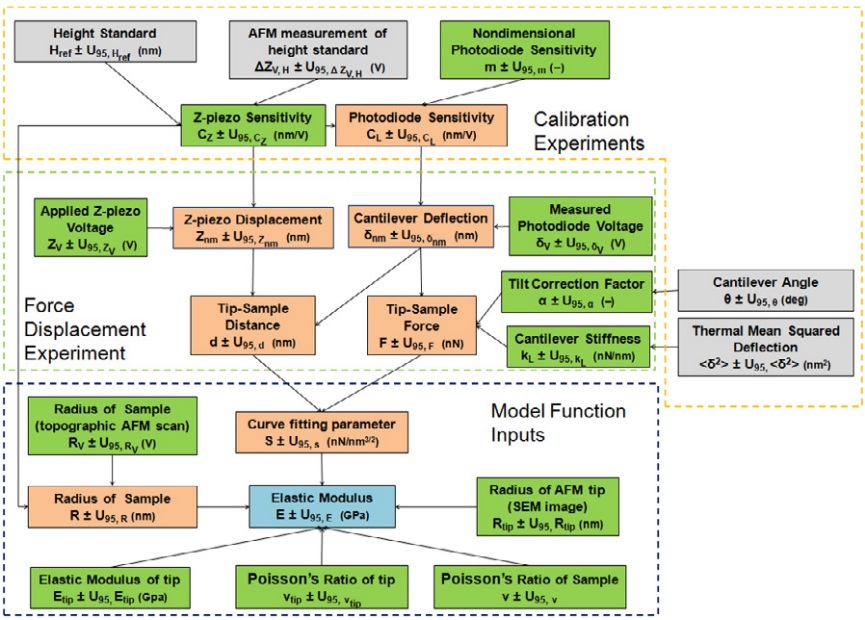

Figure 3. Flow chart representing propagation of uncertainty from inputs to elastic modulus. Uncertainty propagates from a series of input parameters, given in table 1, through a collection of intermediate parameters, to the output of elastic modulus. Different colors represent input parameters, pre-input parameters, intermediate parameters and elastic modulus.

Physikalisch Technische Bundesanstalt with methods traceable to the wavelength of light. The calibrated height value is (7.9 ± 1.1) nm. C_Z was determined to be (14 ± 2) nm V^{-1}. These uncertainty bounds are given for the 95% confidence interval.

The photodiode sensitivity (C_L) was determined by performing F–Z curves on mica in time near (less than 4 min) to the measurement of interest. For calibration, 103 F–Z curves were measured. The slope in the curves (V nm^{-1}) was

determined by fitting a line to the upper half of the contact region. C_L, the inverse of this slope, was determined to be approximately 86 nm V^{-1}.

C_L and C_Z are correlated because C_Z must be used to convert the Z-piezo voltage into displacement. If C_L is chosen as an input to the DRE a term describing the correlation between the uncertainties in C_L and C_Z would need to be included in the uncertainty propagation equation. The correlation between C_L and C_Z can be avoided by defining a new calibration parameter, the nondimensional photodiode sensitivity (m), which is found by performing the calibration F–Z curves with the Z-piezo displacement in units of volts. m is the inverse slope of the calibration F–Z curve (i.e. volts of deflection versus volts of piezo extension curve) in the contact region; in other words, m is the volts of Z-piezo motion per volts of photodiode output. C_L is related to m and C_Z by the equation $C_L = mC_Z$. The calibration result is shown in figure 2(C). m was determined to be 6.1 ± 0.3.

The cantilever stiffness (k_L) was determined by the thermal tuning method [27]. The measurement was performed on a Polytec MSA 4800 laser Doppler vibrometer. The power spectral density of the first resonance peak was measured repeatedly. For calibration, 60 of these curves were recorded and the value of k_L was estimated based on the resulting distribution. k_L was determined to be (2.5 ± 0.1) nN nm^{-1}. This result is shown in figure 2(B). The angle of the cantilever (θ) was determined by measuring the angle of the AFM head and adding the angle of the cantilever holder. The resulting uncertainty was the lowest count of the instrument used to measure the angles. θ was determined to be $(11 \pm 1)^\circ$. If the thermal method is performed using the AFM photodiode instead of a laser Doppler vibrometer the uncertainties in C_Z and m will propagate into the cantilever stiffness.

It is necessary to determine the values and uncertainties of the inputs to the model function. The radius of the AFM tip (R_{tip}) is determined by viewing two orthogonal images of the tip in a scanning electron microscope (SEM). An SEM image of the AFM tip is shown in figure 2(D). R_{tip} was determined to be (10 ± 2) nm. The radius of the CNC (R) was determined from the topography image collected simultaneously with the F–Z data by assuming that the CNC is a cylinder and the height measured in the AFM corresponds to the diameter of this cylinder. R was determined to be approximately 4 nm. Since R was measured with the AFM it is dependent on C_Z and if R was considered as an input to the DRE it would be necessary to include correlation terms in the Taylor series uncertainty propagation formula. This problem can again be circumvented by defining a new model parameter R_V such that R_V is the radius measured in volts. R_V was found to be (0.31 ± 0.04) V. The AFM tip is silicon covered with a 10 nm layer of tungsten carbide. The elasticity of the AFM tip (E_{tip}) and the Poisson's ratio of the tip (ν_{tip}) were assumed to be between the elastic modulus of silicon and the elastic modulus of tungsten carbide and were taken as (300 ± 250) GPa and 0.3 ± 0.1, respectively. This range covers the elastic properties of all crystallographic orientations of silicon [29] and the elastic properties of tungsten carbide [30]. The Poisson's ratio of the CNC (ν) was assumed to be 0.3 ± 0.1.

2.4. Uncertainty propagation

Each observable, calibration factor and model parameter will have an associated uncertainty. These uncertainties must be propagated through the DRE. Several uncertainty propagation techniques can be used to propagate the uncertainty in the observable parameters to the uncertainty in the parameter of interest, such as elastic modulus or work of adhesion. These methods include the Taylor series uncertainly propagation [21], general polynomial chaos [31] and Monte Carlo methods [32]. The final output of this process is a probability distribution function for the model parameter of interest on the analyzed structure. Here we focus on the Taylor series uncertainty propagation and provide a comparison the Monte Carlo method in the supplement (available at stacks.iop.org/Nano/22/455703/mmedia). The Taylor series formula for the uncertainty in the elasticity is given as follows:

$$\begin{aligned} u_E^2 = {} & \left(\frac{\mathrm{d}f_1}{\mathrm{d}Z_{V_1}}u_{V_1}\right)^2 + \cdots + \left(\frac{\mathrm{d}f_1}{\mathrm{d}Z_{V_n}}u_{Z_{V_n}}\right)^2 + \left(\frac{\mathrm{d}f_1}{\mathrm{d}\delta_{V_1}}u_{\delta_{V_1}}\right)^2 \\ & + \cdots + \left(\frac{\mathrm{d}f_1}{\mathrm{d}\delta_{V_n}}u_{\delta_{V_n}}\right)^2 + \left(\frac{\mathrm{d}f_1}{\mathrm{d}C_Z}u_{C_Z}\right)^2 + \left(\frac{\mathrm{d}f_1}{\mathrm{d}m}u_m\right)^2 \\ & + \left(\frac{\mathrm{d}f_1}{\mathrm{d}k_L}u_{k_L}\right)^2 + \left(\frac{\mathrm{d}f_1}{\mathrm{d}\alpha}u_\alpha\right)^2 + \left(\frac{\mathrm{d}f_1}{\mathrm{d}R_V}u_{R_V}\right)^2 \\ & + \left(\frac{\mathrm{d}f_1}{\mathrm{d}R_{tip}}u_{R_{tip}}\right)^2 + \left(\frac{\mathrm{d}f_1}{\mathrm{d}E_{tip}}u_{E_{tip}}\right)^2 + \left(\frac{\mathrm{d}f_1}{\mathrm{d}\nu_{tip}}u_{\nu_{tip}}\right)^2 \\ & + \left(\frac{\mathrm{d}f_1}{\mathrm{d}\nu}u_\nu\right)^2. \end{aligned} \tag{3}$$

The partial derivatives are evaluated numerically with the central difference method. Any uncertainty whose relative uncertainty is more than an order of magnitude smaller than the largest relative uncertainty is neglected.

The methodology described above has ignored all uncertainties associated with the form of the model itself. These uncertainties are called epistemic uncertainties and, if included, would increase the range of the predicted 95% confidence intervals. Examples of epistemic uncertainties include the fact that the DMT model does capture all of the deformation mechanics present in the experiment, the true geometry of the CNC does not match the geometry of the CNC in the experiment, the bottom contact between the CNC and the substrate contributes to the total deformation and the F–Z curve must be shifted in the Z axes such that the location of $d = 0$ matches the DMT model. Uncertainties related to the assumptions about the DMT model and surface geometry can be examined by considering more complicated models. This is outside the scope of this work. Uncertainty associated with the identification of $d = 0$ (contact point) has been addressed by several authors. It has been shown that misidentification of the contact point can lead to significant errors in the predicted elastic modulus [33]. The effect of misidentification of the contact point is further discussed in the supplement (available at stacks.iop.org/Nano/22/455703/mmedia).

3. Materials and methods

Tunicate CNC samples were provided by Professor Christoph Weder of the Université de Fribourg. The preparation of these

crystals is described elsewhere [34]. Tunicate CNCs were chosen because they are nearly 100% crystalline, and they have a larger particle size (8–20 nm in width, 500–4000 nm in length) and a more uniform particle morphology as compared to CNCs from other sources. For AFM work, a 0.1 mg ml^{-1} aqueous CNC suspension was deposited on a mica substrate, excess solution was removed with an absorbent material and the sample allowed to sit in a dry nitrogen ambient (0.1% relative humidity) overnight before imaging.

A Nanotec electronic AFM[6] and a Dulcinea controller (www.nanotec.es; Tres Cantos, Spain) was used to measure F–Z curves on a single, isolated CNC. During imaging the AFM head was placed in an environmental chamber in which the relative humidity was maintained at 0.1% by pumping nitrogen through the chamber. The relative humidity was measured with a relative humidity meter placed about 5 cm from the sample. Team Nanotec HSC 20 cantilevers (www.team-nanotec.de) with a nominal stiffness of 3 N m^{-1} were used for imaging. Image processing and data acquisition were performed in the WSxM (version 4.0) software [35]. It should be noted that this AFM system did not use a closed-loop Z-piezo controller. This means that, to minimize the piezo hysteresis and nonlinearities, the Z-piezo calibration needs to be performed under the same mean Z-piezo voltage and range of motion as the F–Z experiment. This differs from a closed-loop system where highly linear sensors can be used to provide feedback input for the Z-piezo motion to reduce these hysteretic and nonlinear effects.

The force–volume (F–V) mode in the WSxM software was used to acquire simultaneous topography and F–Z data. F–V mode is similar to standard F–Z AFM except that the feedback is turned on between the forward and backward curves to acquire the surface location. Surface location is defined as a set amount of cantilever deflection. F–V mode creates a map of topography and F–Z curves over a specified area. A 128 × 128 pixel map was acquired on the CNC-mica surface over an area 300 by 300 nm. The maximum force for the topography image was 10 nN. Each F–Z curve consists of 125 data points, has a Z ramp range of 30 nm and was acquired at a rate of about 30 Hz per F–Z curve. By creating a simultaneous map of F–Z curves and topography, the precise location of force curve analysis can be determined.

4. Results

Figure 4(A) is a topography map corresponding to a map of 128×128 F–Z curves, showing a section of the analyzed CNC. The F–Z data was confirmed to be elastic by examining the topography before and after the experiment and observing that no changes occurred. The topography of the crystal appears to be homogeneous. The complete description of the procedure for material property extraction is given in the supplement (available at stacks.iop.org/Nano/22/455703/mmedia).

[6] Certain commercial equipment, instruments or materials (or suppliers, software, etc) are identified in this paper to foster understanding. Such identification does not imply recommendation or endorsement by the National Institute of Standards and Technology, nor does it imply that the materials or equipment identified are necessarily the best available for the purpose.

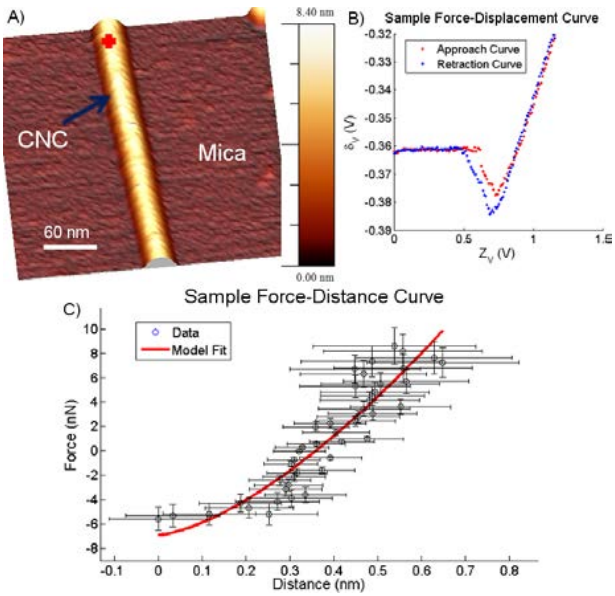

Figure 4. (A) Topography image of Tunicate CNCs deposited on mica. The cross shows location where a sample force–displacement curve was extracted. (B) One sample force–displacement curve extracted from the top of the CNCs. (C) One sample force–distance curve with 95% CI shown for each data point on the curve.

One sample F–Z curve is shown in figure 4(B). The converted F–d curve with the 95% confidence interval for each data pair and the least-squares fit to the DMT model is shown in figure 4(C). For most F–d curves the data is well described by the model fit; however, sometimes the data is not described by the model well due to tip debris, unexpected deformation mechanics or other causes. This data is eliminated by considering only datasets with a goodness of fit parameter, (R^2_{gof}), greater than 0.6.

A series of F–Z curves was extracted from the apex of the CNC crystal for further analysis. Each F–Z curve is used to generate a normal probability distribution for E and W based on the uncertainties associated with elasticity extraction. Each normal probability distribution can be described by a mean value and standard deviation. Out of 122 F–Z curves 85 F–Z curves fit to the DMT model with an R^2_{gof} value greater than 0.6. For each F–Z curve with an R^2_{gof} greater than 0.6 the mean and 95% confidence interval for each probability distribution is shown in figure 5. It remains to convert these 85 probability distributions for E and W into a single probability distribution function describing the total transverse elastic modulus and work of adhesion of the CNC. The total probability distribution of E and W can be constructed by adding together the probability distributions for the individual measurements and renormalizing the result (see the supplement for details available at stacks.iop.org/Nano/22/455703/mmedia). This result is shown in figure 5(D). Based on this formulation the mean modulus is 8.1 GPa and the 95% confidence interval is 2.7–20 GPa. This is in agreement with previous theoretical studies [36]. Similarly the mean value for the total work of adhesion probability distribution is 116 mJ m^{-2} and the 95% confidence interval is 77–180 mJ m^{-2}. It should be emphasized that the predicted

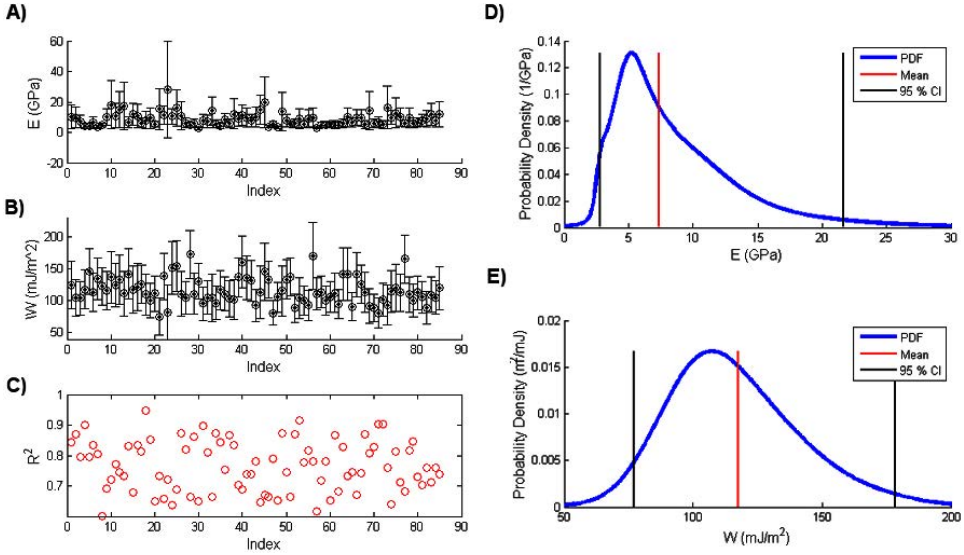

Figure 5. Summary of cellulose nanocrystal transverse elastic modulus and work of adhesion datasets. (A) This shows the mean and 95% confidence intervals for elasticity (E) datasets. (B) This shows the mean and 95% confidence intervals for work of adhesion (W) datasets. (C) R^2_{gof} values associated with the datasets. Points with an R^2_{gof} less than 0.6 have been eliminated. (D) Estimated probability distribution function (PDF) for transverse elastic modulus (E) dataset based on the means and 95% confidence intervals found in (A). The mean value of E is 8.1 GPa and the 95% CI is from 2.7 to 20 GPa. (E) Estimated PDF for work of adhesion (W) dataset. The mean value of W is 116 mJ m^{-2} and the 95% CI is from 77 to 180 mJ m^{-2}.

range for the 95% confidence intervals for E are larger than what would be estimated using experimental replicates. This is because some of the uncertainty associated with the measurement technique is systematic in nature and thus is not captured by experimental replicates.

Table 1 gives the contribution of each input variable to the variance in transverse elastic modulus of a single sample F–Z curve shown in figure 4(B). The description and uncertainty of each input variable is discussed in section 2. The sensitivity of E to each variable is calculated by applying the central difference method to the algorithm for computing the elastic modulus. The contribution of each variable to the variance of E is given as the sensitivity of each variable multiplied by its uncertainty squared. The values with the largest standard combined uncertainties are the Z-piezo sensitivity (C_{Z}), AFM tip radius (R_{tip}) and measured CNC radius (R_{V}). These uncertainties are only known to be within 10% of their reported value. For this single representative F–Z curve the largest uncertainty in E arises from the uncertainty in the nondimensional photodiode sensitivity (m). In the sample dataset shown in figure 4, the 3% uncertainty in the nondimensional photodiode sensitivity accounts for 93% of the 37% uncertainty in the elastic modules. This phenomena occurs because in the DRE two relatively large values (δ_{nm}, Z_{nm}) are subtracted to give a relativity small value (d). m is the only input parameter that shifts δ_{nm} independently of Z_{nm}. This has a large effect on the value of d and hence the predicted value of E.

When considering the reported value of transverse elastic modulus and work of adhesion, it is important to keep in mind the assumptions used in the derivation of the DRE and in the uncertainty propagation methods. Only the uncertainty in the input to the model has been addressed and not the uncertainty in the form of the model itself. The confidence intervals are only valid for comparison of other results that have been computed with the same model. It should be noted that the reported uncertainties are for a single isolated CNC and are not necessarily representative of all CNCs. CNCs will vary from sample to sample and source to source. This work is a first step in investigating such variations.

5. Discussion

The framework described in this paper shows that the uncertainties in extracting the local modulus of the sample are greater than what would be sampled by multiple replicates of the experiments. Taking into account the components of uncertainty arising from a systematic effect in the different calibration factors is important in quantifying the uncertainty in AFM-based nanomechanical measurements. The large uncertainty bounds on measured elastic modulus and work of adhesion values are a cause for concern and we hope our findings will spur new efforts to reduce uncertainty in such measurements. At the same time it must be recognized that we have dealt with nanoparticles with moderate elasticity. As the sample stiffness is reduced and the sample thickness is increased, for example while measuring materials with E less than 1 GPa and more than 100 nm thick, this uncertainty is likely to decrease since larger indentations are possible in the linear elastic regime. However, for CNCs and most other nanoparticles indentations of more than a few nanometers lead to inelastic behavior.

Given the large contribution of m to the measured modulus and work of adhesion, especially on nanoparticles, it is interesting to discuss experimental approaches to decrease uncertainty in m. This is a very important variable that AFM

Table 1. Summary of values and uncertainties for inputs into the elastic modulus data reduction equation for a single sample force–distance curve. The parameters and their uncertainties are described in section 2. This measurement suggests that the value of elastic modulus is 10.2 GPa with a 95% CI ranging from 2.5 to 18.1 (a standard combined uncertainty of 3.9 GPa). These values are for a single F–Z curve and not the entire collection of F–Z curves presented in figure 5(B). The nondimensional photodiode sensitivity (m) is shown to be the dominant contributor to the uncertainty in E, contributing 90% of the variance for this single representative F–Z curve.

Sample uncertainty analysis					
Variable (x)	Description	Value	Standard uncertainty (u_x)	Sensitivity ($\frac{dE}{dx}$)	Variance contribution ($(\frac{dE}{dx}u_x)^2$)
Calibration parameters					
C_Z	Z-piezo sensitivity	14 (nm V^{-1})	1 (nm V^{-1})	0.5 (GPa nm V^{-1})	0.24 (GPa^2)
m	Nondimensional photodiode sensitivity	6.1 (—)	0.15 (—)	25 (GPa)	14 (GPa^2)
α	Tilt correction factor	1.037 (—)	0.007 (—)	10 (GPa)	0.005 (GPa^2)
k_L	Cantilever stiffness	2.5 (nN nm^{-1})	0.1 (nN nm^{-1})	4 (GPa nm nN^{-1})	0.18 (GPa^2)
Model parameters					
R_{tip}	Radius of tip	10 (nm)	1 (nm)	0.4 (GPa nm^{-1})	0.14 (GPa^2)
E_{tip}	Elastic modulus of tip	300 (GPa)	250 (GPa)	0.01 (—)	0.08 (GPa^2)
ν_{tip}	Poisson's ratio of tip	0.3 (—)	0.1 (—)	0.23 (GPa)	0.001 (GPa^2)
R_V	Radius of sample	0.31 (V)	0.04 (V)	6 (GPa V^{-1})	0.04 (GPa^2)
ν	Poisson's ratio of sample	0.3 (—)	0.1 (—)	6 (GPa)	0.4 (GPa^2)
Data pairs sampled during experiment				Mean sensitivity	Total variance contribution
Z_{V_i}	Z-piezo voltage	— (V)	0.001 (V)	30 (GPa V^{-1})	0.09 (GPa^2)
δ_{V_i}	Photodiode voltage	— (V)	0.0003 (V)	170 (GPa V^{-1})	0.33 (GPa^2)
Total				Expanded uncertainty ($k_p = 2$)	Variance
E	Elastic modulus	10.2 (GPa)	4 (GPa)	8 (GPa)	16 (GPa^2)

instrument developers must try to minimize in order to improve quantitative measurements of nanomechanical properties using the AFM. We anticipate many approaches to this challenge will emerge in the near future, but here we discuss a few possibilities:

(1) If the tip–sample gap or indentation (d) were to be directly measured instead of subtracted pointwise from measurements of piezo displacement and cantilever deflection signals, then a major component of this uncertainty could be reduced. Direct measurement of tip–sample gap is a challenging but nonetheless plausible goal using a variety of instrumental techniques and sensors.
(2) Increasing the Z-piezo range of the calibration curve on a hard sample can reduce uncertainty in m: however, several factors need to be considered before this can be taken as a true improvement.
(3) Increasing the cantilever deflection sensitivity or decreasing the deflection noise floor of the AFM system.

We have presented a framework for quantifying uncertainty in local nanomechanical properties measured with AFM F–Z curves. The approach takes into account the largest relevant uncertainties and can be implemented for any AFM system and sample material. In the CNC case study, the input parameters with the largest uncertainties were the Z-piezo sensitivity (C_Z), AFM tip radius (R_{tip}) and measured CNC radius (R_V), each of which was about 10% uncertain. However, it was the nondimensional photodiode sensitivity (m), which was only 3% uncertain, but accounted for most of the uncertainty in E. We do not expect this trend to hold for all levels of force and indentation. For example, when indenting cells indentations of the order of 500 nm are common. In this case the cantilever deflection and Z-piezo position are not as close together and m should not have such a large contribution to uncertainty. It would require a systematic study to identify the exact point at which m ceases to be the dominant parameter, but in the authors' experience this result should hold for indentations of 2 nm or less. The framework has identified the most relevant methods for improving instrumentation and standards to minimize uncertainty in material properties extracted with AFM. In the quest for reliable nanoengineered products, quantifying uncertainty in measured properties of nanomaterials is among the foremost scientific challenges for which the proposed framework provides an important path forward.

Acknowledgments

The authors are grateful to financial support for this research provided by the Forest Products Laboratory under USDA grant: 'Research on Nanotechnology Related to Wood and Wood-based Materials' and Purdue University under Discovery Park Seed Grant: 'Cellulose Nanocrystal Technology: Surface Functionalization and Composite Applications'. The authors also thank Drs D C Hurley

and J Kramar of NIST for their illuminating comments on the manuscript, Professor R Reifenberger (Physics, Purdue) for his valuable guidance on experimental aspects of AFM measurements and Dr C Weder of the Université de Fribourg for providing the tunicate CNC samples.

References

[1] Binnig G and Quate C 1986 *Phys. Rev. Lett.* **56** 930–3
[2] Lee C, Wei X, Kysar J W and Hone J 2008 *Science* **321** 385–8
[3] Zhao Y, Ge Z and Fang J 2008 *Phys. Rev.* E **78** 031914
[4] Lahiji R R, Xu X, Reifenberger R, Raman A, Rudie A and Moon R J 2010 *Langmuir* **26** 4480–8
[5] Palaci I, Fedrigo S, Brune H, Klinke C, Chen M and Riedo E 2005 *Phys. Rev. Lett.* **94** 175502
[6] Perkins M, Ebbens S J, Hayes S, Roberts C J, Madden C E, Luk S Y and Patel N 2007 *Int. J. Pharm.* **332** 168–75
[7] Lucas M, Mai W, Yang R, Wang Z L and Riedo E 2007 *Nano Lett.* **7** 1314–7
[8] Stan G, Ciobanu C V, Parthangal P M and Cook R F 2007 *Nano Lett.* **7** 3691–7
[9] Stan G, Ciobanu C V, Thayer T P, Wang G T, Creighton R J, Purushotham K P, Bendersky L A and Cook R F 2009 *Nanotechnology* **20** 035706
[10] Deng X, Joseph V R, Mai W, Wang Z L and Wu C F J 2009 *Proc. Natl Acad. Sci.* **106** 11845–50
[11] Hiratsuka S, Mizutani Y, Tsuchiya M, Kawahara K, Tokumoto H and Okajima T 2009 *Ultramicroscopy* **109** 937–41
[12] Maivald P, Butt H J, Gould S A C, Prater C B, Drake B, Gurley J A, Elings V B and Hansma P K 1991 *Nanotechnology* **2** 103–6
[13] Hurley D, Kopycinska-Muller M, Kos A and Geiss R 2005 *Meas. Sci. Technol.* **16** 2167–72
[14] Butt H J, Cappella B and Kappl M 2005 *Surf. Sci. Rep.* **59** 1–152
[15] Kim M S and Pratt J R 2010 *Measurement* **43** 169–82
[16] Haycocks J and Jackson K 2005 *Prec. Eng.* **29** 168–75
[17] Wilkening G 2005 *Nanoscale Calibration Standards and Methods* (Weinheim: Wiley–VCH)
[18] Hubbe M A, Rojas O J, Lucia L A and Sain M 2008 *Bioresources* **3** 929–80
[19] Eichhorn S J *et al* 2010 *J. Mater. Sci.* **45** 1–33
[20] Wagner R, Raman A and Moon R 2010 *Proc. 10th Int. Conf. on Wood and BioFiber Plastic Composites, and Cellulose Nanocomposites Symp. (Madison, WI)* pp 309–16
[21] Coleman H W and Steele W G 2009 *Experimentation, Validation, and Uncertainty Analysis for Engineers* (Hoboken, NJ: Wiley)
[22] Capadona J R, Shanmuganathan K, Tyler D J, Rowan S J and Weder C 2008 *Science* **319** 1370–4
[23] Fukuzumi H, Saito T, Wata T, Kumamoto Y and Isogai A 2009 *Biomacromolecules* **10** 162–5
[24] Higgins M, Proksch R, Sader J, Polcik M, Mc Endoo S, Cleveland J and Jarvis S 2006 *Rev. Sci. Instrum.* **77** 0034–6748
[25] Sader J E, Chon J W M and Mulvaney P 1999 *Rev. Sci. Instrum.* **70** 3967–9
[26] Hutter J L and Bechhoefer J 1993 *Rev. Sci. Instrum.* **64** 1868–73
[27] Butt H J and Jaschke M 1995 *Nanotechnology* **6** 1–7
[28] Hutter J L 2005 *Langmuir* **21** 2630–2
[29] Wortman J J and Evans R A 1965 *J. Appl. Phys.* **36** 153–6
[30] Lassner E and Schubert W D 1999 *Tungsten—Properties, Chemistry, Technology of the Element, Alloys, and Chemical Compounds Springer* (Berlin: Springer)
[31] Xiu D and Karniadakis G 2002 *SIAM J. Sci. Comput.* **24** 619–44
[32] Metropolis N and Ulam S 1949 *J. Am. Stat. Assoc.* **44** 335–41
[33] Lin D C and Horkay F 2008 *Soft Matter* **4** 669–82
[34] van den Berg O, Capadona J R and Weder C 2007 *Biomacromolecules* **8** 1353–7
[35] Horcas I, Fernandez R, Gomez-Rodriguez J M, Colchero J, Gomez-Herrero J and Baro A M 2007 *Rev. Sci. Instrum.* **78** 013705
[36] Tashiro K and Kobayashi M 1991 *Polymer* **32** 1516–26

IOPscience iopscience.iop.org

Home Search Collections Journals About Contact us My IOPscience

Uncertainty quantification in nanomechanical measurements using the atomic force microscope

This article has been downloaded from IOPscience. Please scroll down to see the full text article.

2011 Nanotechnology 22 455703

(http://iopscience.iop.org/0957-4484/22/45/455703)

View the table of contents for this issue, or go to the journal homepage for more

Download details:
IP Address: 128.46.220.209
The article was downloaded on 28/12/2011 at 20:09

Please note that terms and conditions apply.